ACS APPLIED MATERIALS & INTERFACES

Letter

Cite This: ACS Appl. Mater. Interfaces 2019, 11, 9679−9684

www.acsami.org

High-Performance Surface Barrier X-ray Detector Based on Methylammonium Lead Tribromide Single Crystals

Qiang Xu,*[,†] Wenyi Shao,[†] Yang Li,[†] Xinlei Zhang,[†] Xiao Ouyang,[‡] Jun Liu,[§] Bo Liu,[∥] Zhengyun Wu,[⊥] Xiaoping Ouyang,*[,†,‡] Xiaobin Tang,[†] and Wenbao Jia[†,#]

[†]Department of Nuclear Science and Engineering, Nanjing University of Aeronautics and Astronautics, Nanjing 211106, China

[‡]Institute of Nuclear and New Energy Technology, Tsinghua University, Beijing 100084, China

[§]Northwest Institute of Nuclear Technology, Xi'an 710024, China

[∥]School of Physics Science and Engineering, Tongji University, Shanghai 200092, China

[⊥]Department of Physics, Xiamen University, Xiamen 361005, China

[#]Collaborative Innovation Center of Radiation Medicine of Jiangsu Higher Education Institutions, Suzhou 215000, China

ABSTRACT: Hybrid methylammonium lead tribromide ($MAPbBr_3$) perovskite has attracted great attention in ionization radiation detection. However, the charge collection remains a challenge. Here, fast response and high-sensitivity X-ray detection based on $MAPbBr_3$ single crystals with a surface barrier Schottky diode has been achieved at room temperature. The Schottky surface barrier can overcome the large leakage current at a high electrical field, enabling us to reduce the noise and increase the charge collection efficiency. This surface barrier device has been demonstrated a 3 times improvement over the photoconductor based X-ray detector, which enables usage in nuclear medicine, especially for X-ray imaging technology.

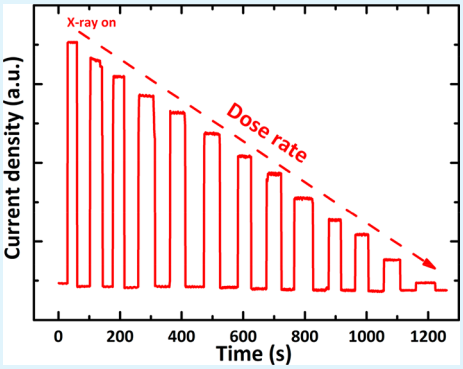

KEYWORDS: *surface barrier, X-ray detector, perovskite single crystal, Schottky diode, fast response*

High-performance, low-cost X-ray detection has attracted much attention, because it offers wide applications for scientific research, medical imaging, home security, nondestructive testing, and so on.[1−4] In order to detect X-ray photons, two strategies have been developed: the indirect method that converts them to UV−visible photons by using scintillators and then converts UV−visible photons to charges by a photodetector; or direct method that converts these X-ray photons into electron−hole pairs, which is dominated by semiconductors.[4] A material that can serve as an efficient direct X-ray detector requires distinct properties: high resistivity, high $\mu\tau$ product, high atomic numbers, and low charge trap density. A high atomic number with high density attenuates the incident X-ray. High purity with low charge density is to avoid charge trapping while performing the single-event analysis. Thus, high-quality semiconductor materials (amorphous Se, high-purity Ge, CdZnTe) have been developed as most successful for commercial X-ray or γ ray detectors.[1−6] In addition, the devices based on these materials are limited by cost, testing conditions, or technology. Therefore, a novel material is pursued to overcome these limitations with good detection performance.

Recently, organic−inorganic methylammonium lead halide perovskite materials $MAPbX_3$ ($MAPbX_3$, where MA = CH_3NH_3, X = Br, I) have received great attrention and have been successfully employed to detect α particles, X-rays, and γ rays by using a direct photon to current conversion method.[7−12] The outstanding performances of these devices are mainly ascribed to $MAPbX_3$ perovskite single crystals (SCs) with low-cost, high atomic and intrinsic properties such as a tunable wide band gap, high mobility−lifetime product, long diffusion length, and low trap density.[13,14] All these ionization radiation detectors based on perovskite materials are sandwich structure photoconductor devices with two ohmic contacts on both sides of the crystals. Charges generated by incident X-ray photons are shifted and collected at metal contacts under the external electric field. However, charge transportation and collection efficiency limit the performances of present photoconductor based devices.[15] Two strategies provide the possibilities to increase the charge collection efficiency: (i) apply a high external electric field to increase the drift length of charge carriers and reduce the charge trapping (but this will also decrease the signal-noise ratio due to the increase of dark current) and (ii) grow high-quality crystals with high resistivity and mobility−lifetime product (but this is always limited by crystal growth technology). In addition, although the photoconductor device has the potential to take good X-ray images, the dark current of the device is hard to

Received: December 10, 2018
Accepted: February 22, 2019
Published: February 22, 2019

DOI: 10.1021/acsami.8b21605
ACS Appl. Mater. Interfaces 2019, 11, 9679−9684

satisfy by the operating conditions of commercial flat-panel X-ray imagers.[5]

The charge collection and leakage current at a high electrical field are a source of electrical noise, which decreases the detection performance. To improve the detection performance, several methods have been tried to overcome these limitations: inserting a layer of brominated (3-aminopropyl)triethoxysilane molecules to reduce the dark current,[10] harvesting the high mobility−lifetime product of single crystals by growing high-quality alloyed perovskite SCs to improve bulk resistivity, and using a guard ring electrode to reduce the surface leakage.[12]

In this study, we have successfully fabricated an X-ray detector based on solution growth $MAPbBr_3$ SCs with surface barrier Schottky structure at room temperature. This structure diode has been employed to overcome charge collection limitations, which consists of Ohmic contact and Schottky contact on both sides of the crystals. The surface Schottky barrier could greatly reduce the surface leakage current at a high electrical field that could enhance the charge collection efficiency. A high-performance surface barrier X-ray detector has been achieved with high sensitivity and fast response time.

All raw chemicals include methylamine (33 wt % in absolute ethanol), hydrobromic acid (47% in water), ethanol, diethyl ether, DMF (anhydrous, 99.8%), and lead bromide ($PbBr_2$, 99.99%), which is a commercial product without further purification. High-quality $MAPbBr_3$ single crystals (SCs) were synthesized by using the inverse temperature crystallization growth method with two steps. First, CH_3NH_3PbBr (MABr) powder was prepared after mixing a molar ratio of methylamine and hydrobromic acid at 0 °C in an ice bath for 1 h. The raw MABr powder was collected after evaporating the solution by using a rotary evaporator. To increase the purity of the MABr powder, the raw MABr powder was washed with ethanol and diethyl ether at least three times. Second, we prepared a saturated precursor solution by dissolving a molar ratio of MABr and $PbBr_2$ into DMF solution at 60 °C. Finally, the high-quality crystals were harvested from the solution after putting the precursor solution in a vial and keeping it in an 80 °C oil bath for 2 days.

The selected raw $MAPbBr_3$ SCs were fabricated with an X-ray detector with a Schottky diode. A 50 nm thick Al layer was deposited onto the surface of crystals in a 1 mm diameter circle through a shadow mask by using sputtering as the Schottky contact. Then the devices were obtained after a 50 nm thick layer of Au was evaporated onto both sides, thus serving as the ohmic electrode.

Single-crystal X-ray diffraction (XRD) was performed using a Bruker D8 Discover X-ray diffraction system. The optical transmission spectrum was characterized by a Cary 5000 UV−vis spectrophotometer. The photoluminescence (PL) spectrum was recorded by an FLS 980 fluorescence spectrometer from Edinburg Instrument, which was excited with a 405 nm laser. The capacitance−voltage measurement was carried out using a KCV-300 capacitance meter with a test frequency of 1 MHz. X-ray photons were coming from a portable X-ray tube (tungsten target) operated at 40 kV. The X-ray dose rate of depended on the operating current of the X-ray tube and was calibrated by a dosimeter. The X-ray generated current was recorded by a Keithley 2400 source meter. To measure the time profile of the device, the collimated X-ray was modulated by a thick steel chopper, and the current was recorded by a lock-in amplifier and oscilloscope (Tektronix DPO71254). The distance between the source and devices is about 2 cm. All measurements were done in air at room temperature.

Large crystals have been harvested from the precursor solution by using the inverse solution growth method that kept the precursor solution in an 80 °C oil bath for several days. The crystal size is around 13.9 mm × 13.8 mm × 2.6 mm (Figure 1a). The crystal structure properties are investigated by single-crystal X-ray diffraction (XRD) measurement at room temperature. Two main peaks located at around 15.4° and 30.4° have been observed, which are ascribed to the (100) and (200) lattice planes, respectively. It reveals that the $MAPbBr_3$ SC is a cubic structure with space group, which is also consistent with the literature.[14,16]

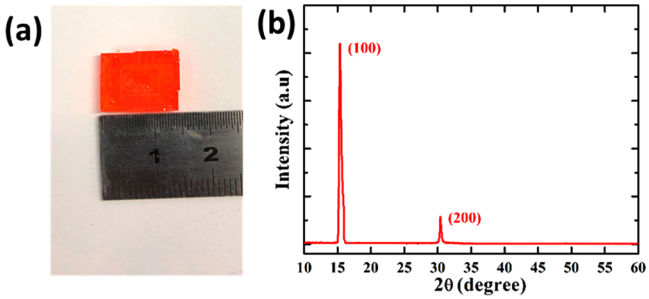

Figure 1. Structure properties of $MAPbBr_3$ SCs. (a) Photograph of as-grown $MAPbBr_3$ single crystal with the dimension of 13.9 mm × 13.8 mm × 2.6 mm. (b) Single-crystal X-ray diffraction pattern of $MAPbBr_3$ single crystal.

Optical properties of the $MAPbBr_3$ SC were evaluated by UV−vis transmission and photoluminescence (PL) spectra, as shown in Figure 2a,b. The optical transmittance of the MAPbBr3 crystal is about 70%, while the wavelength exceeds 570 nm. The optical band gap could be calculated from the cutoff edge by using the Tauc plot: $\alpha h\nu \propto (h\nu - E_g)$, where E_g is the optical band gap, α is the absorption coefficient, and h and ν are the Planck constant and frequency of the incident photon, respectively. The calculated optical band gap is 2.2 eV by extrapolating the linear intercept (the inset of Figure 2a). The PL spectrum exhibits a sharp peak at 566 nm with the full width at half-maximum (fwhm) of 14 nm, which was excited by a 405 nm laser at room temperature in air. The optical band gap and PL spectrum imply that the $MAPbBr_3$ SC is a direct band to band material. Moreover, the high transmission and narrow PL peak indicate this is a high-quality material with low trap density.[17]

Metal−semiconductor contact is a key metric to characterize the device performance. To archive excellent detection performance, Schottky contact between Al and the $MAPbBr_3$ crystal is evaluated by using capacitance−voltage (C−V) measurements operated at 1 MHz (Figure 3). The characterization of the charge collection performance of Schottky diode metrics such as capacitance (C), barrier height, carrier concentration, and applied voltage (V) can be expressed as follows[18]

$$C(V) = A\sqrt{\frac{\varepsilon\varepsilon_0 q^2 N_d}{2(\varphi_0 + qV)}} \quad (1)$$

where A is the area of the diode, ε is the relative permittivity of the semiconductor, ε_0 is the permittivity of vacuum, q is the electron charge, N_d is the concentration of uncompensated

DOI: 10.1021/acsami.8b21605
ACS Appl. Mater. Interfaces 2019, 11, 9679−9684

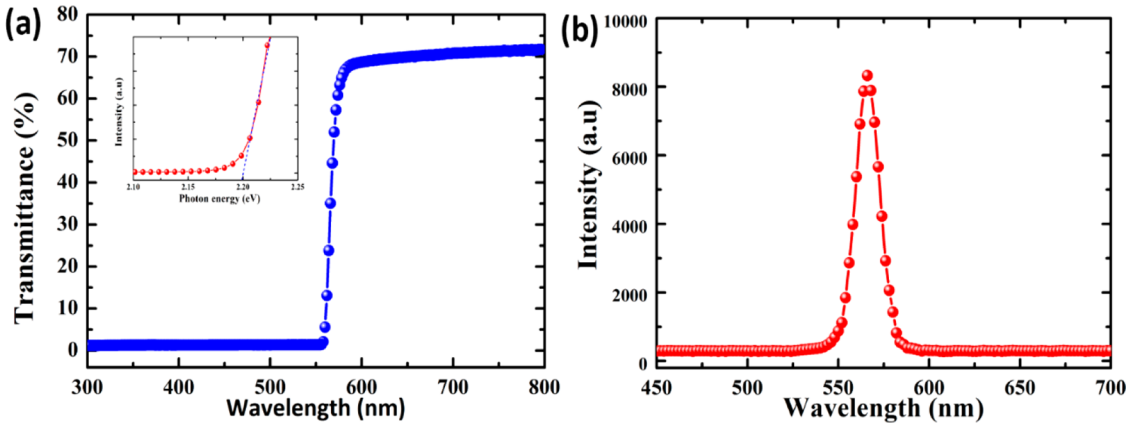

Figure 2. Optical properties of $MAPbBr_3$ SCs. (a) Optical transmission of $MAPbBr_3$ SC. The inset is the Tauc plot of calculated optical bandgap. (b) Photoluminescence spectra of $MAPbBr_3$ SC excited with a 405 nm laser at room temperature.

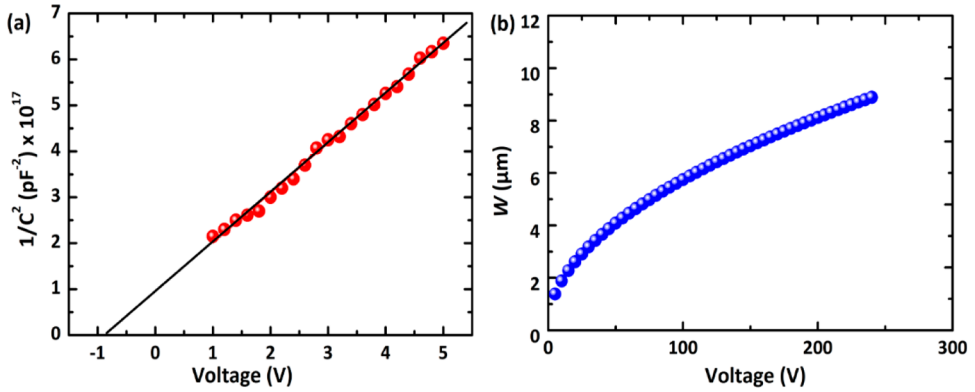

Figure 3. Electrical properties. (a) C^{-2} plot as a function of applied voltage, V. The black line represents the linear fitting. (b) Calculated barrier height width of the depletion layer versus applied voltage.

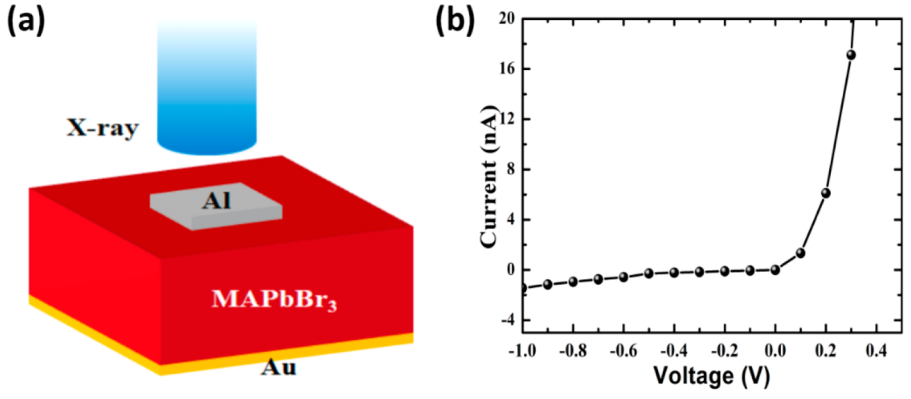

Figure 4. Detector design. (a) Schematic diagram of the $MAPbBr_3$ single crystals perovskite device. (b) Typical current−voltage curve of the Au-$MAPbBr_3$−Al sandwich structure device operating at low voltage and dark atmosphere.

donors. $\varphi_0 = qV_{bi}$ is the barrier height, and V_{bi} is the diffusion (build in) potential. The above equation can also be expressed as

$$C^{-2} = \frac{2}{A^2} \times \frac{V_{bi}}{q\varepsilon\varepsilon_0 N_d} - \frac{2}{A^2} \times \frac{V}{q\varepsilon\varepsilon_0 N_d} \quad (2)$$

$$N_d = \frac{2}{q\varepsilon_0\varepsilon_R A^2 \, d(1/C^2)/dV} \quad (3)$$

Therefore, the barrier height and concentration of uncompensated donors can be obtained from the fitted linear regression, which is plotted as a solid black line on the basis of the above equation, and its intercept with the voltage axis. The obtained V_{bi} and N_d for the diode are 0.83 eV and 8.6×10^{17} cm^{-3}, respectively. Here, the ε_R of the $MAPbBr_3$ material is 25.5.[13,18] Furthermore, the depletion layer width (W) can be calculated using the following equation:[19,20]

$$W = \sqrt{\frac{2\varepsilon\varepsilon_0}{qN_d}(V_{bi} - V)} \quad (4)$$

The calculated W is a function of applied reverse voltage, as shown in Figure 3b. A larger W value can be reached by

DOI: 10.1021/acsami.8b21605
ACS Appl. Mater. Interfaces 2019, 11, 9679−9684

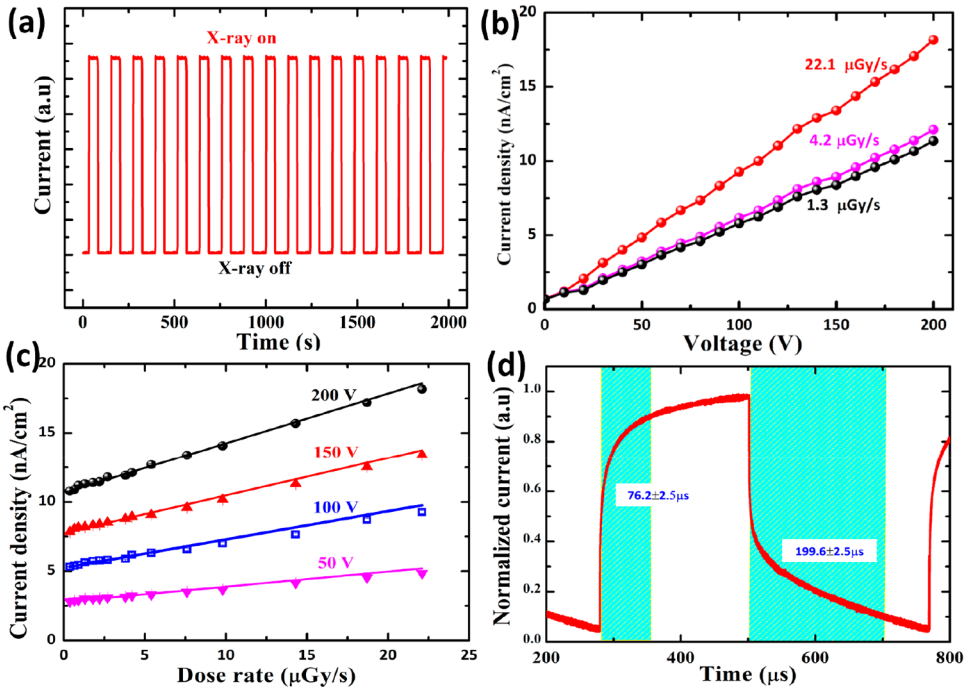

Figure 5. X-ray detection performance. (a) Current responses of devices on and off under a 50 keV X-ray, with a tungsten target. (b) Photocurrent versus applied voltage of the Au/$MAPbBr_3$/Al Schottky radiation detector at various X-ray dose rates for the same device. (c) Photocurrent at various dose rates with different reverse voltages. (d) Transient photoresponse of the detector measured at reverse voltage 200 V, dose rate 22.1 μGy/s. The time response of the devices was measured using a collimated X-ray chopped at 2 kHz.

Table 1. Summary of X-ray Detection Performances for Perovskite-Based X-ray Detector

devices	sensitivity (μC $Gy^{1-}cm^{-2}$)	response time(μs)	X-ray (KeV)	dose rate (μGy/s)	ref
Au/BCP/C60/$MAPbBr_3$/Si	2.1×10^4	255	8	11.8	10
ITO/PI-$MAPbBr_3$(dilute)/MPC/PI-$MAPbI_3$/ITO	1.1×10^{-2}	5×10^4	100	1000	11
Ag/ZnO/PCBM/$MAPbI_3$/PEDOT:PSS/ITO	2.527×10^3	NA	70	6720	25
Au/$MAPbBr_3$/C60/BCP/A	80	216	50	NA	8
Au/poly-TPD/$MAPbBr_3$ PSC/C60 doped PCBM/Ag	2.36×10^4	26	30	100	26
Al/$MAPbBr_3$/Au	359	76.2 ± 2.5	50	22.1	this study
Au/$MAPbBr_3$/Au	62	272 ± 5	50	22.1	this study

increasing the applied reverse voltage. W is approximately 8.1 μm at the reverse voltage of 200 V.

Considering the p-type behavior of $MAPbBr_3$ SCs (demonstrated by CV), high and low work function metals were usually employed to form the Ohmic and Schottky electrodes, respectively. Because of the relative high work function of Au (5.1 eV) and the small work function of Al (4.28 eV), these two metals were chosen to deposit on the surface of crystals as Ohmic and Schottky electrodes.[21,22] To minimize the incident X-ray attenuated by the Al electrode, the evaporated thickness of the Al was about 50 nm. The typical Schottky behavior current−voltage (I−V) curve of the Au/$MAPbBr_3$/Al structure has been observed in Figure 4b.

Obviously, X-ray imaging in nuclear medicine has become a common and effective tool to diagnose and treat patients. A high performance with low dose rate detection and fast response is essential to minimize the dose rate exposure of the patient for decreasing cancer risk, especially for young patients.[23,24] The X-ray generated a strong, producible photocurrent (Figure 5a) that is dependent on the incident X-ray dose rate, as shown in Figure 5b. The devices were stable without obvious degradation, while operating at a reverse voltage of 200 V. The photocurrents of the device under the dose rate at 1.3, 4.2, and 22.1 μGy/s were investigated in this study (Figure 5b). As shown in Figure 5c, a linear relationship between exposure X-ray dose rate and the current response has been observed. The sensitivity of the device at 50, 100, 150, and 200 V are 109, 204, 271, and 359 μC Gy^{-1} cm^{-2}, respectively, which was derived from the slope of the fitted line.

Figure 5c shows the time response of the device operated at 200 V, irradiated with a collimated X-ray that chopped at 2 kHz. The response and recovery time of devices are defined as the time interval between 10% and 90% of the maximum photocurrent, respectively. The value of response time and recovery time are 76.2 ± 2.5 and 199.6 ± 2.5 μs, respectively. The X-ray detection performance of the photoconductor device with Au/$MAPbBr_3$/Au structure has been investigated. The sensitivity and response time of the photoconductor device are 62 μC Gy^{-1} cm^{-2} and 272 ± 5 μs (Table 1), respectively. These values are greatly matched with previous photoconductor values.[10] After comparison between these two structure devices, the sensitivity and response time of the Al/$MAPbBr_3$/Au Schottky device are 3 times higher or faster than those of the photoconductors detector. The enhanced detection performance is mainly attributed to the 4 order increase of the electrical field (1.43×10^7 V/m), compared with that of the previous

DOI: 10.1021/acsami.8b21605
ACS Appl. Mater. Interfaces 2019, 11, 9679−9684

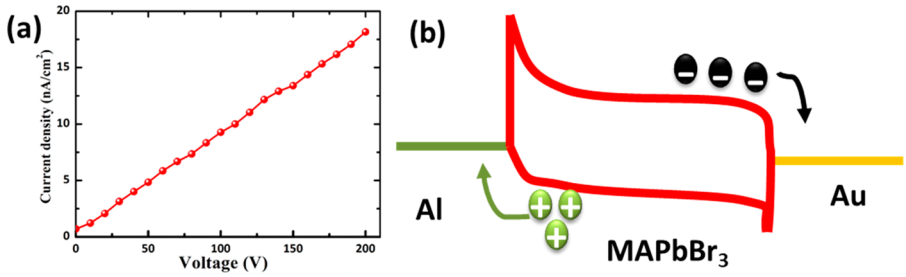

Figure 6. Effect of applied reverse voltage on charge transportation. (a) Current density as a function of applied voltage. (b) Schematic of band diagram of the device under detection mode.

photoconductor device (several hundred V/m).[9,10,27,28] In addition, the leakage current can be greatly suppressed by the barrier between Al and $MAPbBr_3$ SCs.

The observed photocurrent density at 22.1 μGy/s is linearly increasing with the applied voltage (Figure 6a). This is attributed to the charge transportation at various W values. As discussed above, we know that the *W* value is increasing by the applied reverse voltage. The *W* value is 8.1 μm under the reverse voltage of 200 V. Although the *W* value is smaller than the theoretical penetration depth of 50 keV in $MAPbBr_3$ SCs, it is low enough to attenuate the incident 50 keV X-ray. In this case, the current density is increasing linearly with the applied voltage. The dramatically enhanced X-ray detection sensitivity, response, and recovery speed are ascribed to the Schottky barrier between Al and $MAPbBr_3$ SCs. It is because, under the high electrical field, the X-ray generated electron−holes are in the depletion region, which is much faster swept to the metal electrode than the low electrical field (Figure 6b).[20] This will reduce the charge trapping and suppress the carrier recombination and thus increase the charge collection efficiency. When the X-ray beam is switched off, the charges created outside of the depletion region induce longer recovery times.[29]

In conclusion, we have fabricated a reliable, high on−off ratio, fast and sensitive Au-$MAPbBr_3$−Al Schottky sandwich structured X-ray detector with operation in the air at room temperature. The Schottky diode exhibits a built-in barrier height and carrier concentration at 0.83 eV and 8.6×10^{17} cm^{-3}, respectively. At an applied reverse voltage of 200 V, the ratio of photocurrent to dark current is up to 3 orders less than 22.1 μGy/s, the incident X-ray dose rate. The photocurrent density is a linear function of various dose rates under 50 keV X-ray exposure. Thanks to the suppressed leakage current and enhanced charge collections by the surface Schottky barrier, the devices exhibit high sensitivity (359 $\mu C\ Gy^{-1}\ cm^{-2}$) and fast response time (76.2 ± 2.5 μs) at room temperature.

AUTHOR INFORMATION

Corresponding Authors

*E-mail: xuqiangxmu@nuaa.edu.cn (Q.X).
*E-mail: oyxp2003@aliyun.com (O.X).

ORCID

Qiang Xu: 0000-0002-4720-7477
Xiaobin Tang: 0000-0003-3308-0468

Author Contributions

The manuscript was written through contributions of all authors. All authors have given approval to the final version of the manuscript.

Notes

The authors declare no competing financial interest.

ACKNOWLEDGMENTS

This work was funded by the National Natural Science Foundation of China (Grants No. 11705090, 11875166, 11435010 and 11675076). X. Tang acknowledges the support of the National Key Research and Development Program (Grant No. 2016YFE0103600/2017YFC0107700). The authors acknowledge the supported by the National Natural Science Foundation of China (Grant No. 11690040, 11690043) and also thank Dr. Hongying Yang for her expert assistance for further discussion and language polishing.

REFERENCES

(1) Tegze, M.; Faigel, G. X-ray Holography with Atomic Resolution. *Nature* **1996**, *380*, 49−51.
(2) Yaffe, M. J.; Rowlands, J. A. X-ray Detectors for Digital Radiography. *Phys. Med. Biol.* **1997**, *42*, 1−39.
(3) Kapetanakis, E.; Douvas, A. M.; Argitis, P.; Normand, P. Radiation Sensors Based on the Generation of Mobile Protons in Organic Dielectrics. *ACS Appl. Mater. Interfaces* **2013**, *5*, 5667−5674.
(4) Knoll, G. F. *Radiation Detection and Measurement*; JohnWiley, 2010.
(5) Kasap, S.; Frey, J. B.; Belev, G.; Tousignant, O.; Mani, H.; Greenspan, J.; Laperriere, L.; Bubon, O.; Reznik, A.; DeCrescenzo, G.; Karim, K. S. Amorphous and Polycrystalline Photoconductors for Direct Conversion Flat Panel X-Ray Image Sensors. *Sensors* **2011**, *11*, 5112−5157.
(6) Kabir, M. Z.; Kasap, S. O. Charge Collection and Absorption-Limited Sensitivity of X-ray Photoconductors: Applications to a-Se and HgI_2. *Appl. Phys. Lett.* **2002**, *80*, 1664−1666.
(7) Yakunin, S.; Sytnyk, M.; Kriegner, D.; Shrestha, S.; Richter, M.; Matt, G. J.; Azimi, H.; Brabec, C. J.; Stangl, J.; Kovalenko, M. V.; Heiss, W. Detection of X-ray Photons by Solution-Processed Lead Halide Perovskites. *Nat. Photonics* **2015**, *9*, 444−449.
(8) Wei, H.; Fang, Y.; Mulligan, P.; Chuirazzi, W.; Fang, H. H.; Wang, C.; Ecker, B. R.; Gao, Y.; Loi, M. A.; Cao, L.; Huang, J. Sensitive X-ray Detectors Made of Methylammonium Lead Tribromide Perovskite Single Crystals. *Nat. Photonics* **2016**, *10*, 333−339.
(9) Xu, Q.; Wei, H.; Wei, W.; Chuirazzi, W.; DeSantis, D.; Huang, J.; Cao, L. Detection of Charged Particles with a Methylammonium Lead Tribromide Perovskite Single Crystal. *Nucl. Instrum. Methods Phys. Res., Sect. A* **2017**, *848*, 106−108.
(10) Wei, W.; Zhang, Y.; Xu, Q.; Wei, H.; Fang, Y.; Wang, Q.; Deng, Y.; Li, T.; Gruverman, A.; Cao, L.; Huang, J. Monolithic Integration of Hybrid Perovskite Single Crystals with Heterogenous Substrate for Highly Sensitive X-ray Imaging. *Nat. Photonics* **2017**, *11*, 315−321.
(11) Kim, Y. C.; Kim, K. H.; Son, D. Y.; Jeong, D. N.; Seo, J. Y.; Choi, Y. S.; Han, I. T.; Lee, S. Y.; Park, N. G. Printable Organometallic Perovskite Enables Large-Area, Low-Dose X-ray Imaging. *Nature* **2017**, *550*, 87−91.
(12) Wei, H.; DeSantis, D.; Wei, W.; Deng, Y.; Guo, D.; Savenije, T. J.; Cao, L.; Huang, J. Dopant Compensation in Alloyed CH3NH3PbBr3-xClx Perovskite Single Crystals for Gamma-ray Spectroscopy. *Nat. Mater.* **2017**, *16*, 826−833.

DOI: 10.1021/acsami.8b21605
ACS Appl. Mater. Interfaces 2019, 11, 9679−9684

(13) Dong, Q.; Fang, Y.; Shao, Y.; Mulligan, P.; Qiu, J.; Cao, L.; Huang, J. Electron−Hole Diffusion Lengths > 175 μm in Solution-Grown CH3NH3PbI3 Single Crystals. *Science* **2015**, *347*, 967−970.
(14) Liu, Y.; Yang, Z.; Cui, D.; Ren, X.; Sun, J.; Liu, X.; Zhang, J.; Wei, Q.; Fan, H.; Yu, F.; Zhang, X. Two-Inch-Sized Perovskite CH3NH3PbX3 (X = Cl, Br, I) Crystals: Growth and Characterization. *Adv. Mater.* **2015**, *27*, 5176−5183.
(15) Kasap, S. Photodetectors: Low-Cost X-ray Detectors. *Nat. Photonics* **2015**, *9*, 420−421.
(16) Saidaminov, M. I.; Abdelhady, A. L.; Murali, B.; Alarousu, E.; Burlakov, V. M.; Peng, W.; Dursun, I.; Wang, L.; He, Y.; Maculan, G.; Goriely, A. High-Quality Bulk Hybrid Perovskite Single Crystals within Minutes by Inverse Temperature Crystallization. *Nat. Commun.* **2015**, *6*, 7586.
(17) He, Y.; Matei, L.; Jung, H. J.; McCall, K. M.; Chen, M.; Stoumpos, C. C.; Liu, Z.; Peters, J. A.; Chung, D. Y.; Wessels, B. W.; Wasielewski, M. R. High Spectral Resolution of Gamma-rays at Room Temperature by Perovskite CsPbBr3 Single Crystal. *Nat. Commun.* **2018**, *9*, 1609.
(18) Sze, S. M. *Physics of Semiconductor Devices*, 2nd ed.; Wiley-Interscience: New York, 1981.
(19) Clifford, J. P.; Johnston, K. W.; Levina, L.; Sargent, E. H. Schottky Barriers to Colloidal Quantum Dot Films. *Appl. Phys. Lett.* **2007**, *91*, 253117.
(20) Hu, X.; Zhang, X.; Liang, L.; Bao, J.; Li, S.; Yang, W.; Xie, Y. High-Performance Flexible Broadband Photodetector Based on Organolead Halide Perovskite. *Adv. Funct. Mater.* **2014**, *24*, 7373−7380.
(21) Lang, N. D.; Kohn, W. Theory of Metal Surfaces: Work Function. *Phys. Rev. B* **1971**, *3*, 1215.
(22) Green, M. A.; Ho-Baillie, A.; Snaith, H. J. The Emergence of Perovskite Solar Cells. *Nat. Photonics* **2014**, *8*, 506−514.
(23) Brenner, D. J.; Elliston, C. D.; Hall, E. J.; Berdon, W. E. Estimated Risks of Radiation-Induced Fatal Cancer from Pediatric CT. *AJR, Am. J. Roentgenol.* **2001**, *176*, 289−296.
(24) Hall, Eric J.; Giaccia, Amato J. *Radiobiology for the Radiologist*; Lippincott Williams & Wilkins: Philadelphia, 2006; Vol. *6*.
(25) Shrestha, S.; Fischer, R.; Matt, G. J.; Feldner, P.; Michel, T.; Osvet, A.; Levchuk, I.; Merle, B.; Golkar, S.; Chen, H.; Tedde, S. F. High-Performance Direct Conversion X-ray Detectors Based on Sintered Hybrid Lead Triiodide Perovskite Wafers. *Nat. Photonics* **2017**, *11*, 436−440.
(26) Wang, X.; Zhao, D.; Qiu, Y.; Huang, Y.; Wu, Y.; Li, G.; Huang, Q.; Khan, Q.; Nathan, A.; Lei, W.; Chen, J. PIN Diodes Array Made of Perovskite Single Crystal for X-ray Imaging. *Phys. Status Solidi RRL* **2018**, *12*, 1800380.
(27) Pan, W.; Wu, H.; Luo, J.; Deng, Z.; Ge, C.; Chen, C.; Jiang, X.; Yin, W. J.; Niu, G.; Zhu, L.; Yin, L. Cs2AgBiBr6 Single-Crystal X-ray Detectors with a Low Detection Limit. *Nat. Photonics* **2017**, *11*, 726−732.
(28) Intaniwet, A.; Mills, C. A.; Sellin, P. J.; Shkunov, M.; Keddie, J. L. Achieving a Stable Time Response in Polymeric Radiation Sensors under Charge Injection by X-rays. *ACS Appl. Mater. Interfaces* **2010**, *2*, 1692−1699.
(29) Gohil, T.; Whale, J.; Lioliou, G.; Novikov, S. V.; Foxon, C. T.; Kent, A. J.; Barnett, A. M. X-ray Detection with Zinc-Blende (Cubic) Gan Schottky Diodes. *Sci. Rep.* **2016**, *6*, 29535.

DOI: 10.1021/acsami.8b21605
ACS Appl. Mater. Interfaces 2019, 11, 9679−9684